Journal of Nuclear Materials 606 (2025) 155646

Contents lists available at ScienceDirect

Journal of Nuclear Materials

journal homepage: www.elsevier.com/locate/jnucmat

Ab initio study of helium in titanium beryllides

D.V. Bachurin *, C. Stihl, P.V. Vladimirov

Karlsruhe Institute of Technology, Institute for Applied Materials – Applied Materials Physics, Hermann-von-Helmholtz-Platz 1, Eggenstein-Leopoldshafen 76344, Germany

ARTICLE INFO

Keywords:
Ab initio calculations
Titanium beryllides
Helium
Vacancy
Binding energy

ABSTRACT

$Be_{12}Ti$ compound is proposed as a neutron multiplier for tritium-breeding blankets in the demonstration fusion reactor DEMO. Recent experimental studies suggested that $Be_{12}Ti$ could contain additions of other phases such as Be_2Ti and $Be_{17}Ti_2$. In light of these findings, investigation of helium behavior and its binding with vacancy traps in the crystal lattices of these phases is crucial. The paper employs *ab initio* methods to calculate the helium binding energy with various monovacancy types, as well as the helium solution energies at interstitial sites. The solution energy of helium in all non-equivalent interstitial sites of the titanium beryllides is at least 0.6 eV lower than that for pure beryllium. In the titanium beryllides, helium exhibits stronger binding with the titanium vacancy than with the beryllium vacancy. The binding energy of helium to a vacancy in both $Be_{12}Ti$ and $Be_{17}Ti_2$ is almost the same as in pure beryllium, except for Be_2Ti, which has a lower binding energy. When helium is in the vicinity of a vacancy, it causes the displacement of adjacent beryllium atom into the initial vacancy, while helium substitutes the displaced beryllium atom. Some helium atoms may become trapped by a vacancy being outside of it. The obtained results are crucial for the future assessment of interstitial helium diffusion and helium bubble nucleation in titanium beryllides.

1. Introduction

The International Thermonuclear Experimental Reactor (ITER), currently under construction in Cadarache, France, is designed to demonstrate the feasibility of fusion power as a clean and limitless source of energy, paving the way for commercial fusion power plants. The next generation fusion rector, DEMOnstration Power Plant (DEMO), is intended to produce electricity on a commercial scale. DEMO is designed to operate in a harsher environment, with higher temperatures and much higher irradiation doses than those anticipated for ITER. This requires the utilization of advanced neutron multiplier materials capable of operating under extreme conditions with improved properties such as high resistance to oxidation, low tritium retention, low swelling, high melting point, and good compatibility with structural materials.

The modern concept of the DEMO involves the use of beryllium as neutron multiplier material for helium-cooled pebble bed (HCPB) breeding blanket [1]. Neutron multiplication means that when neutrons from hydrogen fusion interact with beryllium, they can produce more neutrons. The latter can interact with lithium ceramics in the breeding blanket to generate tritium, which can be used in the thermonuclear reaction with deuterium. Despite its unique properties, beryllium has some significant drawbacks that severely limit its use in the more extreme conditions of the DEMO reactor. As an alternative to beryllium, intermetallic compounds of beryllium with titanium have been proposed for neutron multiplier material [1].

Authors [2–6] have reported the synthesis and fabrication processes of titanium beryllides on the combination of plasma sintering and rotating electrode methods as well as hot isostatic pressing [7–9]. Recently, ternary compositions of beryllide pebbles [10–14], which include a surface modification process [15], have been proposed to improve binary beryllides.

Beryllides have been suggested for use as a pebble bed [16] or prismatic hexagonal blocks [17]. The HCPB DEMO tritium-breeding blanket requires roughly 400 tons of titanium beryllides, which is comparable to the annual world production of beryllium. As evident from the above, the fabrication of a neutron multiplier in the form of a pebble bed of this size poses substantial challenges and carries a high cost. Consequently, a more cost-effective alternative would be to use hexagonal blocks, which have recently been produced by the Ulba Metallurgical Plant in Kazakhstan and are being investigated at the Karlsruhe Institute of Technology [17,18].

* Corresponding author.
E-mail address: dmitry.bachurin@kit.edu (D.V. Bachurin).

https://doi.org/10.1016/j.jnucmat.2025.155646
Received 12 November 2024; Received in revised form 15 January 2025; Accepted 20 January 2025
Available online 21 January 2025

Based on experimental studies, it has been found that the $Be_{12}Ti$ compound processed by hot isostatic pressing followed by extrusion may contain additions of other phases, such as Be_2Ti, $Be_{17}Ti_2$, pure titanium and beryllium, which do not dissolve completely [8,9]. In addition, some beryllium may evaporate during the manufacturing process, leading to the formation of other phases, even if $Be_{12}Ti$ was the target composition of the powder [10,19]. As a result, during neutron irradiation, tritium accumulation may occur in all these phases, which are always present in the structure in greater or lesser amounts, and subsequently, on its way to the external surface, tritium may have to pass through any of them. Therefore, a significant challenge is to evaluate residual tritium retention and diffusion to assess tritium accumulation after decommissioning of beryllide blocks or pebbles, which is crucial for ensuring operational safety and effective waste management.

Interaction with fast neutrons generates cascades of atomic displacements, leading to the formation of point defects (vacancies, interstitials) and their clusters. When working in the fusion environment, neutron-induced transmutation occurs, associated with the collision of neutrons with atomic nuclei and the subsequent formation of tritium and helium nuclei. These vacancies and vacancy clusters act as traps for tritium and helium atoms thus causing their accumulation in titanium beryllides and formation of bubbles. The continued trapping of tritium and helium results in the growth of these bubbles. In addition, implanted helium can introduce embrittlement in the structure and cause significant internal stress leading to cracking and other forms of damage, as well as changes thermal and mechanical properties of the material [20–25].

Currently, numerous publications deal with the *ab initio* modeling of the helium behavior in the $Be_{12}Ti$ phase [26–28]. The stability of helium-vacancy clusters and the trapping ability of different types of vacancies in $Be_{12}Ti$ for helium atoms have been analyzed in Refs. [27, 28]. In particular, the mechanisms of helium bubble formation by pushing the neighboring beryllium atom into an interstitial position, accompanied by a significant drop in the binding energy, have been established. Thus, an increase in the number of helium atoms absorbed by a vacancy leads to the formation of new vacancies, which in turn increases the number of helium atoms that can be captured by the vacancy complex. Helium atoms remain trapped regardless of their number absorbed by the vacancy cluster. Such self-trapping and trap mutation have also been reported for tungsten [29].

However, to the best of the authors' knowledge, there are currently no studies on the modeling of helium in other phases of titanium beryllides, and issues related to the elucidation of helium behavior in terms of its accumulation remain open and require further research.

The present study employs *ab initio* methods to examine helium behavior in three titanium beryllides (Be_2Ti, $Be_{17}Ti_2$, $Be_{12}Ti$), as well as pure beryllium and titanium. Helium solution energy and binding energy of helium atoms with vacancies are computed, which are essential for analyzing helium retention and release in these materials.

2. Computational methodology

All density functional theory (DFT) computations are carried out using the Vienna Ab-initio Simulation Package (VASP) with the following settings. Brillouin zone sampling is performed using an automatically generated grid with minimal distances of 0.12 $Å^{-1}$ as controlled by the KSPACING-tag, and the set of plane waves includes waves up to 487 eV as regulated by the ENCUT-tag. Further details, in particular on the exact selection procedure of these most important parameters along with an explanation of the measure of accuracy involving total energies of the same crystal structures in different lattices, can be obtained from the appendix and the section on computational technique of our previous publication [30]. Electronic convergence is assumed once the energy difference of subsequent iterations differs by less than 10^{-5} eV as determined by the EDIFF-tag, and ionic convergence is assumed once all forces fall below $5.0{\cdot}10^{-3}$ eV/Å as controlled by the EDIFFG-tag. Smearing of the step at the Fermi level, according to a second order Methfessel-Paxton scheme on a width of 0.2 eV as regulated by the ISMEAR- and SIGMA-tags, results in negligible entropy terms of about 1.0 meV per atom. Projector-augmented wave pseudopotentials [31] are used along with a generalized gradient approximation [32] for the exchange-correlation functional. While all calculations were initially carried out accounting for spin polarization to check for magnetic moments, spin polarization was switched off in subsequent computations whenever possible. Initial structural models of the respective materials are taken from calculations within the Materials Project [33].

Stable interstitial sites for helium are found based on Voronoi tessellations as implemented within pymatgen [34]. To that end, a Voronoi tessellation is computed for all considered materials, yielding Voronoi vertices with sufficient distances to matrix sites and among each other. These are considered candidate interstitial sites for helium and, based on the symmetry operations of the respective material's matrix, equivalent sites are eliminated. For each such non-equivalent candidate site, structural optimizations are carried out using VASP with the parameter set described in the paragraph above, starting from a reasonably sized computational cell containing the ideal crystal of the considered material and an additional helium atom added at the respective site. To preclude premature convergence due to force cancellation from retained symmetries, all structures are perturbed by displacing each atom by 0.01 Å from the equilibrium lattice site into a random direction. After relaxations converged, postprocessing based on resulting stable interstitial sites ensured that only non-equivalent sites were retained. This is achieved by comparing the resulting helium positions to those found in previous calculations as well as their respective equivalent sites due to matrix symmetry operations, only retaining sites with distances larger than 0.01Å.

After obtaining all non-equivalent helium sites under the matrix symmetry operations of the respective material according to the approach described above, monovacancies are considered in addition. For this purpose, first all symmetrically non-equivalent sites in each material are identified, and corresponding monovacancy configurations are structurally relaxed using the VASP. In order to preclude premature convergence due to force cancellation from retained symmetries, all structures are perturbed again by means of atomic displacements of 0.01 Å in random directions. With the reduced sets of symmetry operations of the converged monovacancy configurations, symmetrically non-equivalent sites among all previously obtained stable helium sites were identified, perturbed randomly to destroy all symmetries, and again were structurally relaxed using the VASP. The resulting stable interstitial sites were post-processed, and each site was compared with those obtained in earlier calculations as well as their equivalent sites according to the reduced set of symmetry operations.

3. Results

3.1. Structure and lattice parameters

The present study considers only the α-$Be_{17}Ti_2$ (the space group of $P6_3/mmc$) phase, since the β-$Be_{17}Ti_2$ (the space group of $R\bar{3}m$) is unstable at elevated temperatures and undergoes transformation to the α-$Be_{17}Ti_2$ phase, as specified in the Materials Project [35]. Therefore, for convenience, the α-$Be_{17}Ti_2$ phase will be referred to as $Be_{17}Ti_2$ throughout this paper.

The crystal lattices of titanium beryllides exhibit a higher degree of complexity than the conventional hcp structures of their components, beryllium and titanium. Specifically, the crystal lattice of Be_2Ti (the space group of $Fd\bar{3}m$) accommodates one non-equivalent beryllium site Be1 [16d] (0.375, 0.125, 0.825) and one non-equivalent titanium site Ti1 [8a] (0.75, 0.75, 0.25), as indicated by their Wyckoff symbols in square brackets and fractional coordinates in brackets. The hexagonal

lattice of $Be_{17}Ti_2$ (the space group of $P6_3/mmc$) contains four non-equivalent beryllium sites Be1 [12j] (0.331, 0.37, 0.25), Be2 [12k] (0.164, 0.836, 0.515), Be3 [6g] (0.5, 0.5, 0.5), Be4 [4f] (0.333, 0.667, 0.398), and two non-equivalent titanium sites Ti1 [2b] (0, 0, 0.25) and Ti2 [2d] (0.333, 0.667, 0.75). Similarly, the tetragonal lattice of $Be_{12}Ti$ (the space group of $I4/mmm$) contains four crystallographically non-equivalent sites: three occupied by beryllium Be1 [8f] (0.25, 0.25, 0.75), Be2 [8i] (0.351, 0, 0), Be3 [8j] (0.783, 0, 0.5) and one occupied by titanium Ti1 [2a] (0, 0, 0).

It should be noted that similar atomic positions can become different Wyckoff symbols in various beryllide phases. Therefore, Wyckoff symbols are valid within one particular phase and should not be used for comparison between different phases. Fig. 1 demonstrates the crystal lattices of the titanium beryllides considered in the present study. Due to the complex crystallography of beryllides, it is challenging to visually comprehend their crystal lattices from a two-dimensional format. Therefore, we refer the reader to the supplementary materials of this paper, where three-dimensional models of these crystal lattices are provided for better understanding.

To facilitate the computations, it proves more advantageous to adopt conventional cell configurations. For the $Be_{12}Ti$ compound, a conventional cell with dimensions $1 \times 1 \times 2$ (52 atoms), and for the $Be_{17}Ti_2$, a $1 \times 1 \times 1$ cell (38 atoms) were chosen. Meanwhile, for the Be_2Ti compound, a $2 \times 2 \times 2$ primitive cell (48 atoms) is utilized. This selection ensures a reasonable degree of comparability in terms of computational cell size and total number of atoms across all investigated titanium beryllides. The equilibrium lattice constants and angles are: $a = b = c = 4.539$ Å and $\alpha = \beta = \gamma = 60^\circ$ for Be_2Ti; $a = b = 7.333$ Å, $c = 7.164$ Å, $\alpha = \beta = 90^\circ$, and $\gamma = 120^\circ$ for $Be_{17}Ti_2$; $a = b = 7.324$ Å, $c = 4.151$ Å and $\alpha = \beta = \gamma = 90^\circ$ for $Be_{12}Ti$ (see also Table 1). It is worth noting that the lattice parameters for beryllium, titanium, and $Be_{12}Ti$ compound slightly deviate from those reported in our earlier publications [36,37]. This discrepancy is primarily due to the adoption of an advanced parameter set, specifically the higher plane wave cut-off energy and particularly the denser *k*-point grid. The rationale behind this choice is that the data from the present work are gathered with the intention of developing machine learning-based interatomic potentials in future studies. This requires a dataset with commensurate accuracy in the total energies and forces of structures that include helium, whereas the previously used parameter set was optimized solely for hydrogen.

3.2. Helium at interstitial sites

Since the fastest helium diffusion occurs by the interstitial mechanism, for subsequent calculations of the diffusion characteristics, it is necessary to identify the stable interstitial helium sites in the lattices of the titanium beryllides, between which diffusion occurs by jumping from one stable site to another. In order to compute the helium diffusive properties in the considered titanium beryllides, which will be described in a separate publication, it is crucial to identify all stable non-equivalent interstitial sites for helium atoms. Solution energy is a quantitative measure of how well a solute atom (helium) can be dissolved in a given solvent defined as follows:

$$E_s^X = E^{X+He} - E^X - E_{ref}^{He}, \quad (1)$$

where E^{X+He} and E^X (X = Be, Ti, Be_2Ti, $Be_{17}Ti_2$, $Be_{12}Ti$) are the energies of the computational cell with and without interstitial helium atom, respectively. Here the energy of one helium atom in vacuum, i.e. $E_{ref}^{He} = -0.001$ eV, is used as a reference point.

After performing energy minimization, it turned out that Be_2Ti, $Be_{17}Ti_2$, and $Be_{12}Ti$ phases contain 1, 6, and 4 stable symmetrically non-equivalent interstitial helium sites, respectively. The latter means that helium atoms, initially located in other interstitial sites, will always move to the stable sites during energy minimization. Conversely, both beryllium and titanium contain only two stable interstitial helium sites. In the beryllide phases, the stable interstitial positions for helium were labeled with the capital letters A, B, … F and arranged in order of increasing solution energy, with position A having the lowest solution energy and position F having the highest one. Note that the stable interstitial site A in $Be_{12}Ti$ is not equivalent to the sites A in Be_2Ti and $Be_{17}Ti_2$ due to differences in crystal structure, and the same applies to the other interstitial helium sites.

The following sections present the results for each beryllide separately, with a comparison to available literature data, if applicable. All non-equivalent stable interstitial helium sites for the investigated materials within the computational cells used are shown in Fig. 2 and summarized in Table 2. A three-dimensional representation of the corresponding models is provided in the supplementary materials accompanying this paper.

Table 1
Characteristics of the crystal structures used for *ab initio* modeling of the titanium beryllides and pure beryllium and titanium: the equilibrium lattice parameters a and c (in Å) at 0 K, the number of atoms, N, and the sizes of the computational cells along lattice vectors. The name of the space group and its number are also given.

material	structure	a	c	cell size	N	space group name [group number]
Be	hcp	2.267	3.561	$4 \times 4 \times 2$	64	$P6_3/mmc$ [194]
Ti	hcp	2.923	4.121	$4 \times 4 \times 2$	64	$P6_3/mmc$ [194]
Be_2Ti	cubic	4.539	4.539	$2 \times 2 \times 2$	48	$Fd\bar{3}m$ [227]
$Be_{17}Ti_2$	hexagonal	7.333	7.164	$1 \times 1 \times 1$	38	$P6_3/mmc$ [194]
$Be_{12}Ti$	tetragonal	7.324	4.151	$1 \times 1 \times 2$	52	$I4/mmm$ [139]

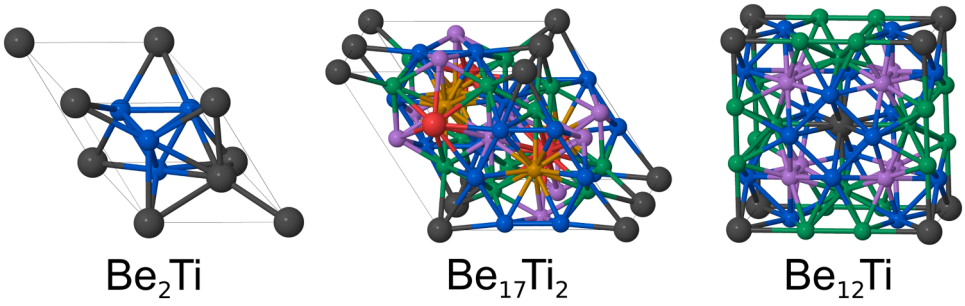

Fig. 1. The crystal structures of the three titanium beryllides under investigation: Be_2Ti (cubic), $Be_{17}Ti_2$ (hexagonal), and $Be_{12}Ti$ (tetragonal). Atoms are colored according to their chemical elements and Wyckoff symbols: large dark grey and red spheres indicate two symmetrically non-equivalent titanium atoms, whereas blue, green, violet and yellow spheres represent four symmetrically non-equivalent beryllium atoms. The conventional unit cells for beryllides are presented. (For a more convenient three-dimensional representation of the crystal lattices, we refer the reader to the supplementary materials accompanying this paper.).

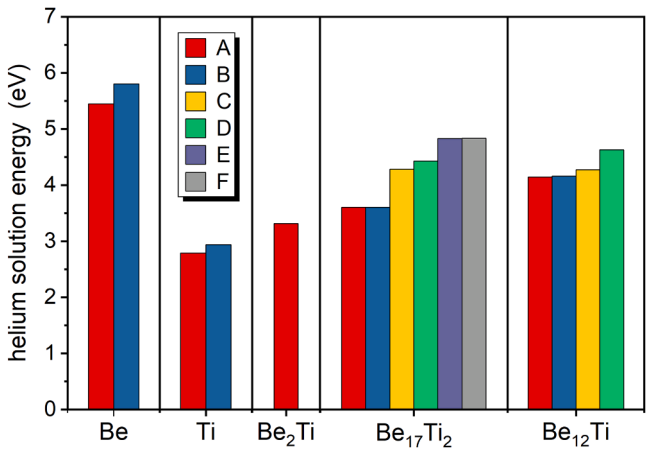

Fig. 2. Solution energies for all non-equivalent stable interstitial helium sites in the titanium beryllides (Be_2Ti, $Be_{17}Ti_2$, and $Be_{12}Ti$) labelled with the capital letters. Notation of letters A-F is explained in the text. Graphical illustration of the results presented in Table 2.

Table 2
Non-equivalent stable interstitial sites for a single helium atom labeled with capitalized letters (A-F) and sorted in order of increasing solution energy, E_s (in eV), calculated at 0 K with Eq. (1) for the three studied titanium beryllides (Be_2Ti, $Be_{17}Ti_2$, and $Be_{12}Ti$) as well as for pure beryllium and titanium. The abbreviations in brackets refer to basal-split mixed (BS_m) dumbbell, basal octahedral (BO), and basal tetrahedral (BT). A dash in a column means that this stable interstitial site does not exist in a particular material. For comparison, the lower part of the table presents the available data on stable interstitial helium obtained in other studies.

material	A	B	C	D	E	F
Be	5.45(BS_m)	5.81(BO)	–	–	–	–
Ti	2.79(BT)	2.94(BO)	–	–	–	–
Be_2Ti	3.31	–	–	–	–	–
$Be_{17}Ti_2$	3.60	3.60	4.29	4.43	4.83	4.84
$Be_{12}Ti$	4.14	4.16	4.27	4.63	–	–
Be [38]	5.62	5.71	–	–	–	–
Be [39]	5.39	5.74	–	–	–	–
Be [40]	5.43	5.64	–	–	–	–
$Be_{12}Ti$ [26]	4.03	4.38	4.53	4.87	–	–

Be and *Ti*. In beryllium, two stable non-equivalent sites for interstitial helium have a relatively high solution energy. The most energetically favorable site is the basal-split mixed dumbbell with a solution energy of 5.45 eV. At that, the helium atom is in the basal plane and displaces one of the nearest beryllium atoms from its equilibrium lattice site in one of the three equivalent directions $\langle\bar{1}100\rangle$, but both atoms remain in the same basal plane. Thus, the helium atom is not exactly in the basal tetrahedral position but is slightly shifted from the center of a triangle. The second stable position for interstitial helium is the basal octahedral site with the solution energy of 5.81 eV, where helium is in an octahedral channel and at the center of a square formed between two adjacent basal planes by four beryllium atoms. In this case, helium remains within the basal plane and only slightly displaces the neighboring beryllium atoms.

Titanium also has two stable interstitial helium sites with solution energies significantly lower than those in beryllium. The basal tetrahedral site is found to be the most energetically favorable one with a solution energy of 2.79 eV, while the second stable interstitial site is the basal octahedral one with a slightly higher solution energy of 2.94 eV.

The data obtained above for the solution energy of the interstitial helium in pure beryllium correspond well with the results of Ganchenkova et al. [41]. The authors [42] have obtained the identical ground-state configuration using Quantum-ESPRESSO code. Note that Vladimirov and Möslang [39] have reported four stable interstitial helium sites in beryllium: the two additional positions, namely, non-basal crowdion and basal-tetrahedral. It is important to note that in Refs. [38–40], three additional stable interstitial helium sites, including octahedral, crowdion and basal crowdion sites, have been revealed in a perfect beryllium lattice, apart from those indicated in Table 2. However, helium atoms in these additional sites have limited stability, and even small deviations can cause displacement to one of two stable positions suggesting that these sites may represent saddle points between the stable configurations.

Be_2Ti. The only stable interstitial helium site located in the tetrahedron formed by two Be1 [16d] atoms and two Ti1 [8a] atoms is revealed. At this site, helium has the lowest solution energy of 3.31 eV as compared to the other stable interstitial helium sites in the $Be_{17}Ti_2$ and $Be_{12}Ti$ compounds (see Table 2). The helium atom is offset from the center of the tetrahedron and is close to the imaginary line connecting the two Ti1 [8a] atoms. Currently, no other works that deal with studying stable interstitial helium sites in Be_2Ti have been published.

$Be_{17}Ti_2$. The six non-equivalent stable interstitial helium sites were found with solution energies ranging from 3.60 to 4.84 eV. At the most energetically favorable interstitial site A, helium is in the middle between two Ti1 [2b] atoms and at the center of the hexagon formed by six Be4 [12k] atoms. The stable interstitial site B is slightly above the hexagon of Be4 [12k] atoms, so the distance between the sites A and B is quite small and equal to 0.3 Å. In this case, the helium atom is closer to one of the Ti1 [2b] atoms but is located on the line connecting the two neighboring Ti1 [2b] atoms. At the third stable interstitial site C with the noticeably higher solution energy of 4.28 eV, the helium atom is inside a pyramid with a rhombus base formed by two Be3 [12j] and two Be4 [12k] atoms and with a vertex at the Ti1 [2b] atom. Note that the helium atom is slightly above its base. At the stable interstitial site D, the helium atom is also in the pyramid with the same quadrangular base formed by two Be3 [12j] and two Be4 [12k] atoms, but with a different vertex at the Ti2 [2d] atom and has the solution energy of 4.43 eV. Thus, the stable sites C and D are on opposite sides of this quadrangular base. At the stable site E, the helium atom is in a tetrahedron formed by two Be1 [4f] and two Be3 [12j] atoms and has the solution energy of 4.83 eV, but as in the cases above, the helium atom is not at the geometric center of this tetrahedron, but close to the line connecting two Be1 [4f] atoms. Helium atom located at the stable interstitial site F has the highest solution energy of 4.84 eV and is very close to site E. The difference between the sites E and F is that the helium atom in site F is in a neighboring tetrahedron, which is also formed by two Be1 [4f] and two Be3 [12j] atoms. It should be noted that in $Be_{17}Ti_2$ there are six such tetrahedra containing interstitial helium positions close to each other. This fact suggests easy diffusion jumps between these positions based on the short jump length. We are not aware of any publication that considers interstitial helium in this titanium beryllide phase.

$Be_{12}Ti$. The four non-equivalent stable interstitial helium sites were found with solution energies in the range of 4.14 and 4.63 eV. The lowest solution energy is at the interstitial site A, when helium is inside a tetrahedron formed by four Be2 [8i] atoms being not at the center of this tetrahedron, but closer to the middle of one of its edges. Since chemically inert helium does not form chemical bonds with beryllium atoms, it should not be equidistant to all neighboring atoms to have a minimum energy. Helium atom can easily have a stable configuration outside the center of the tetrahedron, being closer to any of the atoms forming this tetrahedron. At the second interstitial site B, the solution energy of helium atom is practically equal to that at the most energetically favorable site A. The distance between A and B stable sites of helium is relatively small and equal to 0.5 Å. At the site Be, helium atom is in the plane of a triangle formed by two Be2 [8i] atoms and one Be3 [8j] atom. At the interstitial site C, helium atom is above the plane exactly at the center of the quadrangle formed by the four Be3 [8j] atoms with the vertex at the titanium atom Ti1 [2a]. In other words, site C is inside a pyramid with a square base of beryllium atoms. At the fourth stable interstitial site D,

the solution energy is significantly higher than in sites A-C (see Table 2). The stable site D is in the plane of a triangle formed by Be2 [8i], Be3 [8j], and Ti1 [2a] atoms. There are Be1 [8f] atoms on either side of the apex of this triangle. Thus, the stable site D is in a tetrahedron formed by Be1 [8f], Be2 [8i], Be3 [8j], and Ti1 [2a] atoms.

It should be noted that the solution energies of interstitial helium in the crystal lattices of the three titanium beryllides are much higher than the corresponding solution energies of the hydrogen atom calculated earlier in Ref. [30]. In addition, the difference between the minimum and maximum solution energy of interstitial helium for each beryllide is not as large as for hydrogen.

3.3. Trapping of helium in a monovacancy

The binding energy is a quantitative characteristic used to determine how strongly helium atom is bonded to a monovacancy V (where V = Be1, Be2, Be3, Be4, Ti1, Ti2), which can be determined using the following formula:

$$E_b^X = E^{X+V} + E^{X+He} - E^{X+V+He} - E^X, \quad (3)$$

where E^{X+V+He} represents the energy of the computational cell with a monovacancy V and one helium atom; E^{X+V} represents the energy of the cell with a monovacancy V; E^{X+He} represents the lowest energy configuration containing one helium atom at an interstitial site in material X (where X = Be, Ti, Be_2Ti, $Be_{17}Ti_2$, $Be_{12}Ti$), which is taken as a reference point; E^X is the total energy of the perfect lattice corresponding to the material X. Following this sign convention, positive binding energy indicates attraction, while negative binding energy indicates repulsion between a monovacancy and a helium atom.

A summary of the data obtained for beryllium and titanium as well as for three titanium beryllides is provided in Fig. 3. The binding energies of helium atom located in different non-equivalent sites within the computational cell containing a monovacancy are plotted against the sequential configuration index. In this specific context, the binding energies are arranged in descending order along the horizontal axis, and the configuration index just numbered them without any additional physical meaning. The materials under study exhibit different number of non-equivalent interstitial helium sites, and for these reasons, we use a normalized index along the horizontal axis to scale the results to the same range. Higher binding energy usually indicates the presence of helium in a vacancy, whereas increase in distance from a vacancy typically correlates with a decrease in binding energy.

The results for each titanium beryllide are presented in separate subsections, and when applicable, compared with published data. Fig. 4 visually represents all non-equivalent vacancies and their next-nearest shell atomic environment in the studied materials. Transparent spheres indicate positions of the removed atoms to denote vacancies more clearly. For the sake of clarity and avoid overloading the figure, only interstitial helium sites with positive binding energies are depicted. The coloring of helium atoms is determined by their binding energy with the vacancy, as calculated using expression (3). The red color corresponds to the maximum binding energy, while the white represents zero binding energy.

Note that this visualization is merely schematic and intended to illustrate how helium atoms are situated near the initial vacancy position. This is due to the tendency of helium to displace neighboring beryllium atoms, and in some cases, even titanium atoms, to a lesser degree because of the large difference in atomic mass. As a result of this displacement, a vacancy may develop in an adjacent lattice site. In addition, the figure omits certain helium atoms that possess low binding energy and are located far from a vacancy. However, these stable helium sites are discussed in the corresponding subsection.

In many cases, the helium atom within the investigated vacancies may possess numerous stable sites close to each other. Due to their proximity, no significant energy barrier is expected between them.

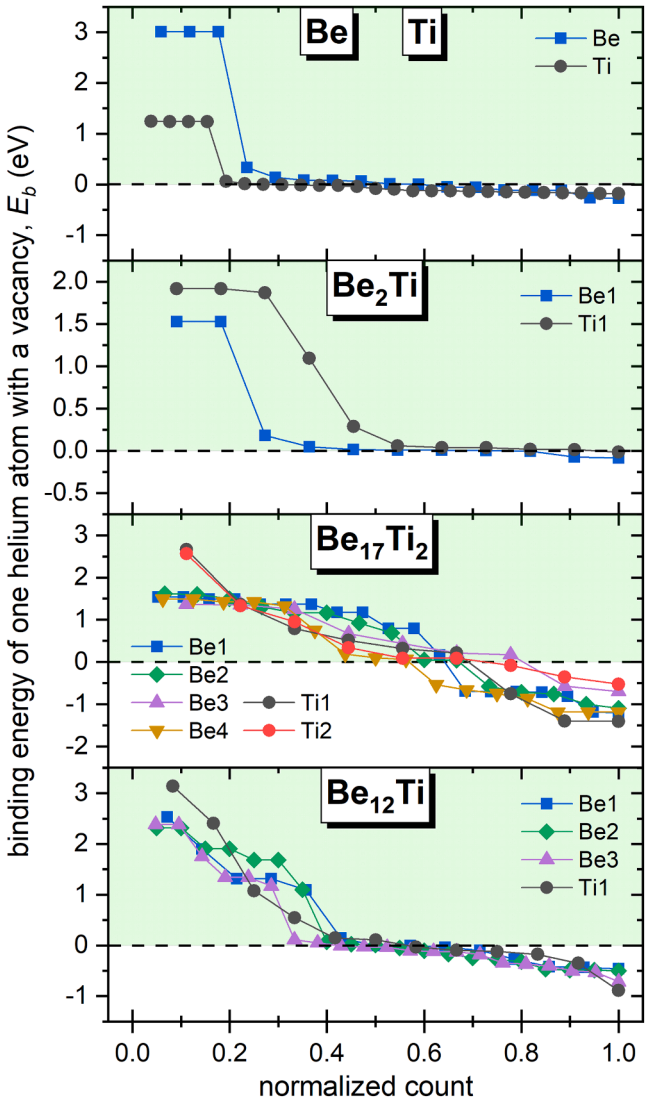

Fig. 3. Binding energy of a single helium atom located in all stable non-equivalent sites within different types of monovacancies in the titanium beryllides (Be_2Ti, $Be_{17}Ti_2$, $Be_{12}Ti$). Helium is situated within a vacancy as well as in all non-equivalent interstitial sites outside it within the computational cell. Stable non-equivalent sites are arranged in descending order of their binding energy. A normalized count is used along the horizontal axis to aid comparison of results. The area with positive binding energies, i.e., where the helium atom is bound to a vacancy, is displayed in light green.

Most of the structures representing non-equivalent stable helium sites both inside and outside the monovacancies in the titanium beryllides are sufficiently complex to be shown in a two-dimensional representation, therefore for a better perception, the reader is referred to the three-dimensional structures included in the supplementary materials to this paper.

3.3.1. Be and Ti

There exists only one type of symmetrically non-equivalent vacancy in hcp beryllium and titanium, which is Be1 and Ti1, respectively. The number following the vacancy type corresponds to that introduced in paragraph 3.1. Although these two elements share an hcp crystal lattice, they have distinct stable interstitial helium sites both within and outside the vacancy.

Be1 vacancy. Within a vacancy, there is only one stable site for helium located at the center of the vacancy and equidistant from the neighboring beryllium atoms. This site has a maximum binding energy

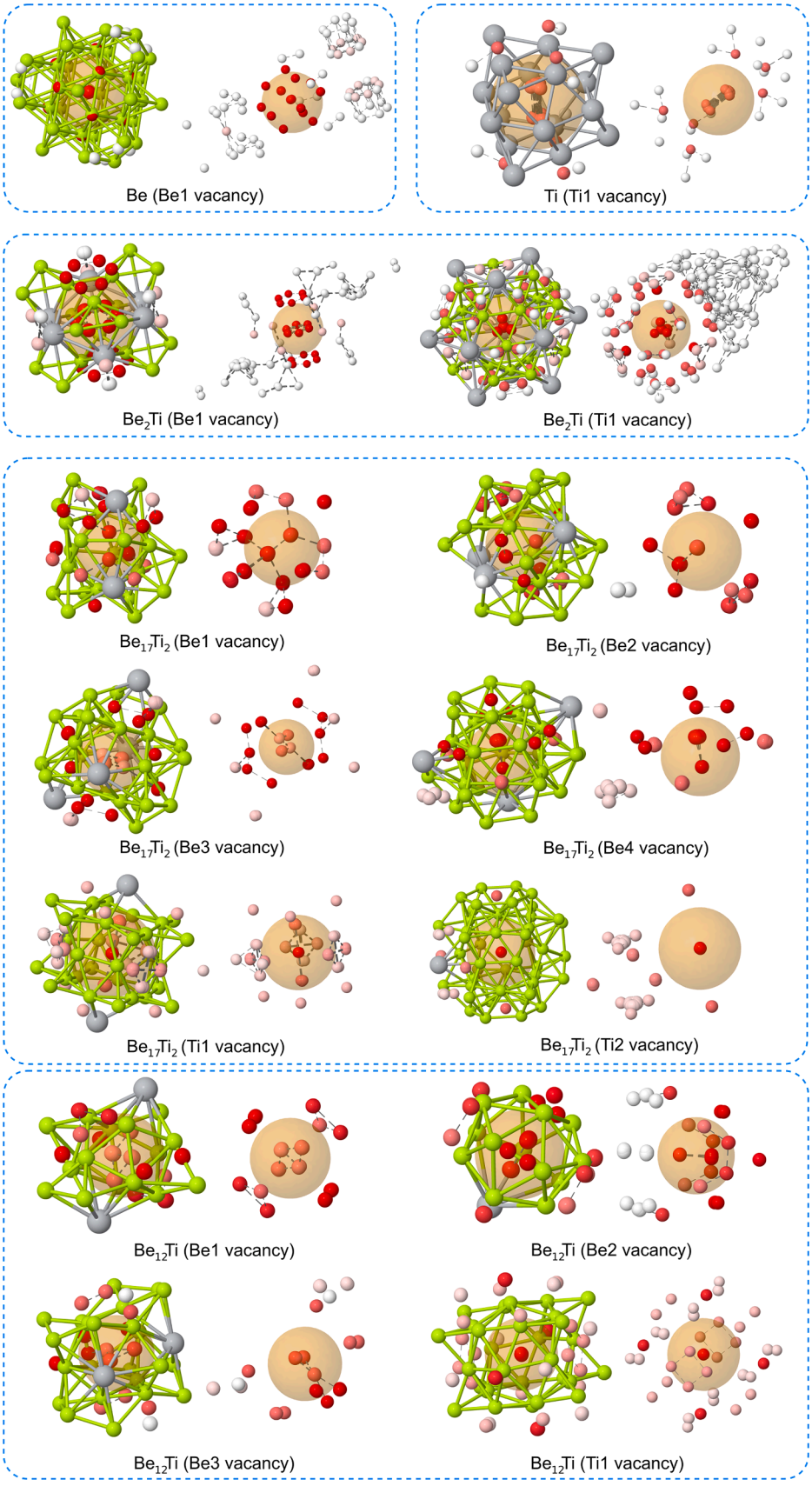

(caption on next page)

Fig. 4. The atomic environment in the next-nearest shell for all non-equivalent types of monovacancies in the titanium beryllides (Be_2Ti, $Be_{17}Ti_2$ and $Be_{12}Ti$) and hcp beryllium and titanium. A transparent sphere centered on the removed atom represents a vacancy. Helium atoms are color coded according to their binding energy, as determined by expression (3). Only helium sites with positive binding energies, indicating an attraction between the vacancy and helium, are visualized. Helium sites with negative binding energies, both inside and outside the vacancies, are intentionally hidden. Beryllium atoms are uniformly colored in light green regardless of their equivalence in the crystal lattice, while titanium atoms with larger radii are depicted in gray.

of 3.01 eV. Our calculations elucidate the recombination mechanism of interstitial helium with a vacancy which appears to be common for nearly all materials considered in this paper. Such a mechanism resembles a short replacement chain usual for the recombination of self-interstitial atoms with vacancy [43]. Being close to a vacancy, interstitial helium displaces neighboring beryllium into the vacancy and takes its place. These beryllium atoms closest to the vacancy are displayed in two colors (light green and red) in Fig. 4, demonstrating that the initial position of the beryllium atom and the position occupied by helium after energy minimization coincide. In other cases, when the helium atom is at a larger distance from the center of the vacancy, its behavior becomes like that in a defect-free lattice, where it forms a basal mixed dumbbell. The binding energies of such complexes range from 0.10 to 0.33 eV, being significantly lower than those found at the center of the vacancy.

Ti1 vacancy. Inside the vacancy, there are two regions where helium atom has stable positions with equal binding energies of 1.24 eV. Each region has 13 equivalent equilibrium sites that are close to each other and have the same binding energies. Such a large number of stable helium positions in a titanium vacancy is due to its larger volume compared to beryllium. As in the case of pure beryllium, when helium atom is close to a vacancy, the helium pushes a titanium atom out of its equilibrium lattice site into the center of the vacancy and occupies one of the stable sites within the newly formed vacancy. Further away from the vacancy, there are also other stable helium sites with negligible binding energies ranging from 0.02 to 0.06 eV. It is noteworthy that the displacement of titanium atoms is markedly less than that of beryllium.

Beryllium and titanium share the same type of crystal lattice. However, since the vacancy volume (approximately equal to the atomic volume in a perfect lattice) of titanium is about 2.16 times the vacancy volume of beryllium, these metals have different stable helium sites. Inside a beryllium vacancy, there is only one stable helium site, while inside a titanium vacancy, there are six such stable sites (see Fig. 4). At the same time, the binding energies of helium atoms that are outside of a vacancy, are quite low for both metals.

3.3.2. Be_2Ti

This beryllide compound has two non-equivalent vacancy types: one Ti1 and one Be1.

Be1 vacancy. Inside the vacancy, there are six equivalent stable sites with equal binding energies of 1.53 eV for the helium atom, forming a regular hexagon with a side of 1 Å. Like in the cases of pure beryllium and titanium, being close to a vacancy, interstitial helium displaces a neighboring beryllium atom, causing it to move to the center of the original vacancy. Thus, the helium appears to be inside the newly created vacancy. In the remaining non-equivalent helium sites with binding energies ranging from 0.02 to 0.18 eV, the presence of helium results in only local displacements of atoms, which, in this case, are insufficient to cause migration of the vacancy.

Ti1 vacancy. The stable helium site, located at the center of the vacancy, has a binding energy value of 1.92 eV. Near this central site, there are four equivalent stable helium sites with a slightly lower binding energy of 1.87 eV, so these four sites form a regular tetrahedron with a side length of 0.85 Å, and the central stable helium site described above is located exactly at the center of this tetrahedron. This stable helium site is equidistant (2.65 Å) from the neighboring titanium atoms. When helium is close to a vacancy (there are four such positions), it moves to the above stable site with a binding energy of 1.87 eV shifting towards the center of the original vacancy. Outside the vacancy, there are stable sites with a binding energy of 1.1 eV, where it causes only a local displacement of neighboring atoms, but no vacancy migration. The binding energy of helium at the remaining sites outside of a Ti1 vacancy is in the range of 0.06 to 0.29 eV.

3.3.3. $Be_{17}Ti_2$

This beryllide contains six non-equivalent vacancy types: four beryllium vacancies (Be1, Be2, Be3, Be4) and two titanium (Ti1 and Ti2) vacancies.

Be1 vacancy. Within this vacancy, there exist two stable helium sites with binding energies of 1.17 and 1.37 eV. These sites are not situated at the center of the vacancy but are closer to the neighboring titanium atom. Additionally, stable sites with a maximum binding energy of 1.53 eV and slightly lower energy of 1.48 eV exist outside of the original vacancy, causing the displacement of neighboring beryllium atoms and forming a vacancy at a new location. The remaining stable helium sites with lower binding energies ranging from 0.16 to 1.37 eV result in only local displacement of beryllium atoms.

Be2 vacancy. There exist two stable helium sites inside the original vacancy. The first, with the highest binding energy of 1.62 eV, is located near two titanium atoms, and the second, with a lower binding energy of 1.16 eV, is on the opposite side of the vacancy. Fig. 4 also shows two helium sites located outside the vacancy and directly on the bond between two beryllium atoms. Again, during energy minimization, the neighboring beryllium atom moves, and a vacancy is formed at a new position. Outside the vacancy, there is only one stable site with a relatively low binding energy of 0.5 eV. Like in the previous cases, stable helium sites with high binding energy are preferentially located near neighboring titanium atoms.

Be3 vacancy. For this vacancy, there are seven non-equivalent helium sites with positive binding energy. The highest binding energy of 1.37 eV is observed for the helium atom, which is located outside this vacancy, as shown in Fig. 4. However, as mentioned above when the energy is minimized, the helium displaces a nearby beryllium atom and ultimately settles in the center of a new vacancy. Inside the vacancy, four stable helium sites exist – two of which are non-equivalent and have binding energies of 0.44 and 0.67 eV. Moreover, the stable site with a higher binding energy of 0.67 eV is closer to the titanium atom. The helium in the remaining stable sites, located outside the vacancy, has binding energies between 0.17 and 0.21 eV.

Be4 vacancy. Inside the vacancy, there are two stable helium sites. The first one, with a binding energy of 1.49 eV, is located near the titanium atom, at the center of a hexagon formed by beryllium atoms. The second site, consisting of multiple closely spaced sites with a slightly lower binding energy of 1.42 eV, is located slightly higher in the plane of the neighboring hexagon of beryllium atoms. Fig. 4 reveals other stable helium sites with a binding energy of 1.49 eV situated outside the vacancy, that are equivalent to the site inside the vacancy near the titanium atom. There are six equivalent helium sites next to a beryllium atom with a binding energy of 1.32 eV. The other three equivalent sites have a binding energy of 0.75 eV. Outside the vacancy, there are also stable helium sites located between two beryllium atoms, with low binding energies ranging from 0.06 to 0.1 eV.

Ti1 vacancy. There are three stable helium sites located within the vacancy. The vacancy center contains the stable helium site with a maximum binding energy of 2.66 eV. Additionally, there are two other stable helium sites inside the vacancy with a lower binding energy of 1.36 eV, which are located between the vacancy center and the neighboring titanium atoms. In stable sites with lower binding energies ranging from 0.31 to 0.79 eV, helium atoms settle into the vacancy due

to the displacement of neighboring beryllium atoms. Other stable helium sites exist outside the vacancy with a relatively low binding energy of 0.21 eV.

Ti2 vacancy. Similar to the previous scenario, there is a single stable helium site at the center of this vacancy with a binding energy of 2.57 eV, which is similar to that found for the Ti1 vacancy. Above and below, there are two stable sites located in the middle of the hexagon formed by beryllium atoms, flanked by two adjacent titanium atoms. These two sites have a lower binding energy of 1.3 eV. There exist other stable helium sites outside the vacancy. Between two titanium atoms there is a cluster of closely located stable sites with binding energies ranging from 0.1 to 0.34 eV. Outside the vacancy, there are three stable helium sites with a binding energy of 0.95 eV, forming an equilateral triangle with a side length of 3.43 Å, with a titanium atom at the center.

3.3.4. $Be_{12}Ti$

Taking the lattice symmetry into account, there are three non-equivalent vacancies on beryllium sites (Be1, Be2, Be3) and one vacancy on titanium sites (Ti1).

Be1 vacancy. Inside the vacancy, there are four stable helium sites in the same plane, forming a rhombus with a side length of 1.17 Å. The two stable sites are located along the long and short diagonals of the rhombus with binding energies of 1.31 and 1.09 eV, respectively. Only in two cases with the highest binding energies of 2.53 and 1.91 eV, a migration of a neighboring beryllium atom into the original vacancy is observed, resulting in the formation of a new adjacent vacancy. In other cases, no migration of the vacancy is observed. The stable interstitial site with the lowest binding energy of 0.14 eV is located at a larger distance from the vacancy.

Be2 vacancy. There are only two stable helium sites within the vacancy, with a maximum binding energy of 2.32 eV and a slightly lower one of 1.91 eV. Additionally, the position with the highest binding energy represents multiple sites located close to each other with the same energy, which can be seen in Fig. 4 as overlapping atomic spheres. Both sites are on a line passing through the titanium and beryllium atoms. On the same line, but outside the vacancy, there exists an interstitial helium site with a binding energy of 1.91 eV, which is equivalent to that located inside the vacancy. This is since this atom causes a displacement of the neighboring beryllium atom, which moves to the center of the original vacancy, and the helium atom occupies the same site next to the titanium atom as in the vacancy. Outside the vacancy, there are stable helium sites with very low binding energies of 0.07 and 0.02 eV. The presence of helium in these sites does not induce the migration of the vacancy. In all other scenarios, the beryllium atom is displaced to the original vacancy.

Be3 vacancy. There exist three stable triangle-forming helium sites in the vacancy. In two of these sites, the binding energy is 1.76 eV, while in one it is 1.34 eV. Helium atoms located closer to the titanium atoms possess a higher binding energy with the vacancy. The sites with the highest binding energy of 2.39 eV are located outside the original vacancy and cause a shift of neighboring beryllium atoms, leading to the formation of a vacancy in one of its neighboring beryllium sites. In all cases where helium atom has a binding energy with a vacancy greater than 1.17 eV, the neighboring beryllium atoms are displaced. However, only in two sites located outside of the vacancy, the helium atoms have the binding energies of 0.05 and 0.11 eV, thereby causing insignificant displacements of neighboring beryllium atoms when they move to their minimum energy site.

Ti1 vacancy. The stable helium site with the highest binding energy of 3.14 eV is located at the center of the vacancy. The four equivalent sites with a binding energy of 2.41 eV are situated outside the original vacancy in the plane formed by six beryllium atoms as shown in Fig. 4. When the binding energy of helium with a vacancy is greater than 0.54 eV, a vacancy is formed in an adjacent beryllium site, accompanied by a shift of the neighboring beryllium atoms. Outside of the vacancy, there are only two stable helium sites with binding energies of 0.11 and 0.15 eV, located at a greater distance from the original vacancy, whereas no shift of neighboring beryllium atoms is observed.

4. Discussion

The behavior of helium in metallic matrices is determined by the repulsive forces between the closed electron shell of helium and the free electrons of the metal. This repulsion arises because the electron cloud of helium resists overlapping with electron density of the metal, requiring additional space to minimize such interactions. As a result, helium atoms are more energetically stable in interstitial sites with larger distances from surrounding atoms and, hence, larger interstitial volumes. This behavior not only determines helium's site preferences within the lattice, but also affects its mobility, thereby influencing the material's properties under irradiation or high temperature exposure.

In addition to interstitial positions, vacancies are energetically favorable helium traps. In contrast to hydrogen, which was studied earlier in Ref. [30], the behavior of helium near a vacancy in titanium beryllides is fundamentally different. The configurations with helium close to a vacancy but outside are unstable. Thus, energy minimization causes the displacement of a neighboring beryllium (or even titanium) atom into the center of the original vacancy and the formation of a vacancy at the position from which this atom originated. The interstitial helium moves into the newly created vacancy. Thus, the recombination of interstitial helium with a vacancy occurs via a short replacement chain. Furthermore, the probability of such collective motion increases as the initial position of a helium atom moves closer to the vacancy.

Zhu et al. [28] studied the stability of helium-vacancy clusters and analyzed the trapping ability of all four types of vacancies in $Be_{12}Ti$ for helium atoms. It has been observed that a single helium atom has binding energies of 1.22, 2.13, 1.30, and 3.09 eV with Be1, Be2, Be3, and Ti1 vacancies, respectively. These values agree well with this study (see SubSection 3.3.4). However, no specific information regarding the location or multiplicity of stable helium sites within a vacancy has been provided in the cited work. The authors note that helium atoms are consistently located closer to the center of vacancies in the $Be_{12}Ti$ phase, indicating its stronger ability to trap helium atoms.

We are only aware of one publication by Wang et al. [27] which reports the presence of two stable helium sites with binding energies of 1.79 and 2.13 eV in only one Be2 vacancy type of bulk $Be_{12}Ti$. This coincides well with the findings above. However, the authors of the cited paper found slightly different values for the shift of the stable helium sites relative to the center of the vacancy. The observed quantitative differences seem to be primarily due to a larger computational cell, together with higher cut-off energy and a denser *k*-point mesh implemented in the present work.

The binding energy of helium with a vacancy in pure beryllium is higher than that with a beryllium vacancy in titanium beryllides, while the binding energy of helium with a titanium vacancy in titanium beryllides is consistently higher than with a beryllium vacancy (see Fig. 3). Despite this, the steady-state concentration of titanium vacancies in $Be_{12}Ti$ under irradiation can be significantly lower than that of beryllium vacancies. In the absence of threshold displacement energies for each element in the alloy, one can use empirical correlations. In particular, the formation energy of titanium vacancies is approximately twice as large as that of beryllium vacancies in titanium beryllides. Since formation energy determines the thermal equilibrium concentration of vacancies, it is reasonable to assume that most of the vacancies formed during irradiation are beryllium vacancies, while titanium vacancies are essentially nonexistent. Therefore, in titanium beryllides, helium is predominantly trapped at beryllium vacancies. This suggests that helium retention in titanium beryllides is predominantly influenced by beryllium vacancies. Since the binding energy of helium with vacancies is lower in titanium beryllides than in pure beryllium, the helium release from titanium beryllides will occur at lower temperatures.

Our results can be compared qualitatively with the experimental

data. Thermal-programmed desorption was performed to measure tritium and helium retention in titanium beryllide Be-7at.%Ti and pure beryllium subjected to neutron irradiation within the HIDOBE irradiation program [44,45]. The specimens contained coarse $Be_{12}Ti$ grains embedded in a beryllium matrix. It was found that the temperature corresponding to the first helium release peak from Be-7Ti is comparable to that observed for pure beryllium. It important to note that the titanium beryllide used in this study consists of a mixture of beryllide phases $Be_{12}Ti$, $Be_{17}Ti_2$, and Be_2Ti embedded in a beryllium matrix [44,45], which complicates the experimental analysis of the contributions of pure beryllium and titanium beryllide phases to helium release. Consequently, its thermal desorption spectrum is expected to resemble a weighted sum of the spectra from these pure phases. This behavior highlights the impact of the material's microstructure on helium trapping and release properties.

It is worth noting that the study [44] also revealed that the tritium and helium release peaks from pure beryllium occur at similar temperatures, while tritium release begins at a lower temperature. This can be explained to some extent by the significantly higher binding energy of helium with beryllium vacancy (≈3 eV) compared to hydrogen (≈1.1 eV) [30].

The solution energies calculated in this work imply the following sequence of helium solubility from lower to higher values: Be < $Be_{12}Ti$ < $Be_{17}Ti_2$ < Be_2Ti < Ti. If diffusion is not a limiting factor and the interphase boundaries are transparent, helium would diffuse from pure beryllium into $Be_{12}Ti$ or other phases with higher titanium content.

The creation of vacancies by knocking atoms out of the respective crystal sublattice is inversely proportional to the threshold displacement energy for that sublattice. Although the energy required for this dynamic process is known to be much higher than the formation energy of Frenkel pairs (i.e. vacancy-interstitial pairs) in equilibrium, it is intuitively clear that they should be correlated. Thus, knowing that in the Be-Ti alloy, the formation energy of the titanium vacancy is higher than that of the beryllium vacancy [30], one can deduce that the concentration of titanium vacancies will be lower under irradiation. Therefore, the effect of higher helium binding to titanium vacancies is compensated by their lower concentration in beryllium alloys under irradiation.

5. Conclusions

Ab initio techniques were utilized to investigate helium behavior in three titanium beryllides (Be_2Ti, $Be_{17}Ti_2$, $Be_{12}Ti$) and their pure components: titanium and beryllium. The binding energies with monovacancies and the energies of helium being dissolved at interstitial sites were calculated. The following are the primary findings.

The helium solution energies in the interstitial sites of the titanium beryllides are at least 0.6–2.1 eV lower than those in pure beryllium. This implies that helium atoms dissolve more easily in the beryllides than in beryllium and that the solution energy increases with increasing beryllium concentration in the alloy.

The calculated solubilities indicate that a multiphase Be-Ti alloy subjected to neutron irradiation should contain varying concentrations of interstitially dissolved helium, with the highest concentration in Be_2Ti, followed by $Be_{17}Ti_2$ and the lowest in $Be_{12}Ti$.

In pure materials, the helium binding energy to the beryllium vacancy is roughly three times higher than that of titanium. On the contrary, among the three titanium beryllides studied, helium binds more strongly to the titanium vacancy than to the beryllium vacancy.

The highest binding energy of helium to a vacancy in $Be_{12}Ti$ and $Be_{17}Ti_2$ is very close to that in pure beryllium, with the exception of Be_2Ti, which suggest a lower helium concentration in this phase compared to the others.

The primary characteristic of helium's behavior in the vicinity of a vacancy in examined materials is the displacement of neighboring beryllium atoms into the original vacancy, which subsequently forms a neighboring vacancy containing a helium atom. This process is referred to as a short replacement chain.

Some helium atoms are weakly bound by a vacancy at intermediate distances, without triggering a replacement chain.

The data obtained for stable interstitial sites will be further used to calculate the helium diffusivity in titanium beryllides which is of great importance in assessing tritium retention.

CRediT authorship contribution statement

D.V. Bachurin: Writing – review & editing, Writing – original draft, Visualization, Validation, Investigation, Formal analysis, Data curation, Conceptualization. **C. Stihl:** Writing – original draft, Visualization, Validation, Methodology, Formal analysis, Data curation. **P.V. Vladimirov:** Writing – review & editing, Validation, Supervision.

Declaration of competing interest

The authors declare that they have no known competing financial interests or personal relationships that could have appeared to influence the work reported in this paper.

Acknowledgements

This work has been carried out within the framework of the EUROfusion Consortium, funded by the European Union via the Euratom Research and Training Programme (Grant Agreement No 101052200 — EUROfusion). Views and opinions expressed are however those of the author(s) only and do not necessarily reflect those of the European Union or the European Commission. Neither the European Union nor the European Commission can be held responsible for them. High performance computing resources were provided by the EUROfusion and performed at the High Performance Computers Marconi-Fusion (Bologna, Italy).

Supplementary materials

Supplementary material associated with this article can be found, in the online version, at doi:10.1016/j.jnucmat.2025.155646.

Data availability

The authors do not have permission to share data.

References

[1] P. Vladimirov, D. Bachurin, V. Borodin, V. Chakin, M. Ganchenkova, A. Fedorov, M. Klimenkov, I. Kupriyanov, A. Moeslang, M. Nakamichi, T. Shibayama, S. Van Til, M. Zmitko, Current status of beryllium materials for fusion blanket applications, Fusion Sci. Technol. 66 (1) (2014) 28–37.
[2] Y. Fujii, M. Miyamoto, J.H. Kim, M. Nakamichi, N. Murayoshi, H. Iwakiri, Hydrogen retention behavior of beryllides as advanced neutron multipliers, Nucl. Mater. Energy 9 (2016) 233–236.
[3] J.H. Kim, H. Iwakiri, T. Furugen, M. Nakamichi, Synthesis and reactivity of single-phase Be17Ti2 intermetallic compounds, Fusion Eng. Des. 102 (2016) 44–49.
[4] J.H. Kim, H. Iwakiri, M. Nakamichi, Reactivity with water vapor and hydrogen storage capacity of Be2Ti compound, Int. J. Hydrog. Energy 41 (21) (2016) 8893–8899.
[5] J.H. Kim, M. Nakamichi, The effect of sintering time on synthesis of plasma sintered beryllides, J. Nucl. Mater. 442 (1–3) (2013) S461–S464.
[6] M. Nakamichi, J.H. Kim, K. Yonehara, Novel granulation process of beryllide as advanced neutron multipliers, Fusion Eng. Des. 88 (6–8) (2013) 611–615.
[7] P. Kurinskiy, V. Chakin, A. Moeslang, R. Rolli, A.A. Goraieb, H. Harsch, E. Alves, N. Franco, Characterisation of titanium beryllides with different microstructure, Fusion Eng. Des. 84 (7–11) (2009) 1136–1139.
[8] R. Gaisin, V. Chakin, M. Duerrschnabel, R. Rolli, T. Weingaertner, A. Goraieb, P. Vladimirov, Effect of HIP at 800 and 900 °C on microstructure and properties of extruded Be-Ti composites, Nucl. Mater. Energy 24 (2020) 100771.
[9] R. Gaisin, V. Kuksenko, M. Duerrschnabel, V. Chakin, A. Goraieb, P. Vladimirov, Effect of HIP at 1000-1200 °C on microstructure and properties of extruded Be-Ti composites, Nucl. Mater. Energy 30 (2022) 101128.
[10] J.H. Kim, M. Nakamichi, Comparative study on arc-melted and plasma-sintered beryllides, J. Alloy Compd. 546 (2013) 171–175.

[11] J.H. Kim, M. Nakamichi, Preliminary synthesis and mechanical property of titanium beryllide pebbles with different chemical compositions, J. Alloy Compd. 585 (2014) 63–68.
[12] J.H. Kim, M. Nakamichi, Synthesis and characteristics of ternary Be-Ti-V beryllide pebbles as advanced neutron multipliers, Fusion Eng. Des. 109 (2016) 1764–1768.
[13] M. Nakamichi, J.H. Kim, K. Ochiai, Beryllide pebble fabrication of Be-Zr compositions as advanced neutron multipliers, Fusion Eng. Des. 109 (2016) 1719–1723.
[14] J.H. Kim, M. Nakamichi, Fabrication and characterization of Be-Zr-Ti ternary beryllide pebbles, Fusion Eng. Des. 136 (2018) 864–868.
[15] M. Nakamichi, J.H. Kim, Prevention of hydrogen generation reaction with water vapor by surface modification of beryllides as advanced neutron multipliers, Fusion Eng. Des. 124 (2017) 905–909.
[16] M. Zmitko, P. Vladimirov, R. Knitter, M. Kolb, O. Leys, J. Heuser, H.C. Schneider, R. Rolli, V. Chakin, S. Pupeschi, L. Magielsen, A. Fedorov, Y. Poitevin, Development and qualification of functional materials for the European HCPB TBM, Fusion Eng. Des. 136 (2018) 1376–1385.
[17] F.A. Hernandez, P. Pereslavtsev, G.M. Zhou, B. Kiss, Q.L. Kang, H. Neuberger, V. Chakin, R. Gaisin, P. Vladimirov, L.V. Boccaccini, G.A. Spagnuolo, S. D'Amico, I. Moscato, Advancements in the helium-cooled pebble bed breeding blanket for the EU DEMO: holistic design approach and lessons learned, Fusion Sci. Technol. 75 (5) (2019) 352–364.
[18] R. Gaisin, V. Chakin, P. Vladimirov, F.A. Hernandez, S. Udartsev, A. Vechkutov, M. Kolmakov, Industrial-scale manufacturing experience of titanium beryllide block for DEMO blanket application, Fusion Eng. Des. 161 (2020) 111862.
[19] R. Gaisin, V. Chakin, R. Rolli, J. Hoffmann, H. Leiste, T. Bergfeldt, U. Jantsch, M. Klimenkov, J. Lorenz, A. Goraieb, P. Vladimirov, A. Moslang, Synthesis of Be12Ti compound via arc melting or hot isostatic pressing, J. Alloy Compd. 818 (2020) 152919.
[20] H.T. Lin, B.A. Chin, Helium-induced weld cracking in austenitic and martensitic steels, J. Mater. Sci. 26 (8) (1991) 2063–2070.
[21] S. Li, M.L. Grossbeck, Z. Zhang, W. Shen, B.A. Chin, The effect of helium on welding irradiated materials, Weld. J. 90 (1) (2011) 19s–26s.
[22] C.A. Wang, M.L. Grossbeck, B.A. Chin, Threshold helium concentration required to initiate cracking during welding of irradiated stainless-steel, J. Nucl. Mater. 225 (1995) 59–68.
[23] S. Agarwal, A. Bhattacharya, P. Trocellier, S.J. Zinkle, Helium induced microstructure damage, nano-scale grain formation and helium retention behaviour of ZrC, Acta Mater. 163 (2019) 14–27.
[24] Y.Q. Ding, J. Pencer, E. Torres, Atomistic simulation study of the helium effects on the deformation behavior in nickel bicrystals, J. Nucl. Mater. 516 (2019) 247–254.
[25] W.Z. Han, M.S. Ding, Z.W. Shan, Cracking behavior of helium-irradiated small-volume copper, Scr. Mater. 147 (2018) 1–5.
[26] X.L. Zhu, C.L. Wang, J.J. Liu, X.M. Zhang, H.Q. Deng, W.S. Duan, L. Yang, Retention and diffusion of transmutation H and He atoms in Be12Ti: first-principles calculations, RSC Adv. 8 (62) (2018) 35735–35743.
[27] Y.L. Wang, C.L. Wang, Z.C. Meng, J.T. Liu, Y.H. Li, L. Yang, Aggregation of retained helium and hydrogen in titanium beryllide Be12Ti: a first-principles study, RSC Adv. 11 (55) (2021) 34860–34869.
[28] X.L. Zhu, Y.W. Zhang, W. Tang, Z.C. Meng, W.T. Li, J.J. Zhang, J. Tang, First-principles study of helium-vacancy complexes in Be12Ti, Phys. Lett. A 424 (2022) 127841.
[29] J. Boisse, C. Domain, C.S. Becquart, Modelling self trapping and trap mutation in tungsten using DFT and Molecular dynamics with an empirical potential based on DFT, J. Nucl. Mater. 455 (1–3) (2014) 10–15.
[30] D.V. Bachurin, C. Stihl, P.V. Vladimirov, Ab initio study of hydrogen in titanium beryllides, Comput. Mater. Sci. 231 (2024) 112419.
[31] G. Kresse, D. Joubert, From ultrasoft pseudopotentials to the projector augmented-wave method, Phys. Rev. B 59 (3) (1999) 1758–1775.
[32] J.P. Perdew, K. Burke, M. Ernzerhof, Generalized gradient approximation made simple, Phys. Rev. Lett. 77 (18) (1996) 3865–3868.
[33] A. Jain, S.P. Ong, G. Hautier, W. Chen, W.D. Richards, S. Dacek, S. Cholia, D. Gunter, D. Skinner, G. Ceder, K.A. Persson, Commentary: the materials project: a materials genome approach to accelerating materials innovation, APL Mater. 1 (1) (2013) 011002.
[34] S.P. Ong, W.D. Richards, A. Jain, G. Hautier, M. Kocher, S. Cholia, D. Gunter, V. L. Chevrier, K.A. Persson, G. Ceder, Python materials genomics (pymatgen): a robust, open-source python library for materials analysis, Comput. Mater. Sci. 68 (2013) 314–319.
[35] The Materials Project: 2024 https://materialsproject.org/.
[36] D.V. Bachurin, P.V. Vladimirov, Ab initio study of Be and Be12Ti for fusion applications, Intermetallics 100 (2018) 163–170 (Barking).
[37] D.V. Bachurin, C. Stihl, P.V. Vladimirov, Ab initio study of hydrogen diffusion in Be and Be12Ti for fusion applications, Comput. Mater. Sci. 187 (2021) 109921.
[38] P.B. Zhang, J.J. Zhao, B. Wen, Vacancy trapping mechanism for multiple hydrogen and helium in beryllium: a first-principles study, J. Phys. Condens. Mater 24 (9) (2012) 095004.
[39] P.V. Vladimirov, A. Moeslang, Ab initio static and molecular dynamics studies of helium behavior in beryllium, J. Nucl. Mater. 442 (1–3) (2013) S694–S698.
[40] Y.L. Wang, C.L. Wang, Z.C. Meng, Y.W. Liu, J.T. Liu, Y.H. Li, L. Yang, Influence of hydrogen and helium nucleation on the mechanical properties of beryllium by first-principles calculations, Nucl. Mater. Energy 31 (2022) 101181.
[41] M.G. Ganchenkova, P.V. Vladimirov, V.A. Borodin, Vacancies, interstitials and gas atoms in beryllium, J. Nucl. Mater. 386-388 (2009) 79–81.
[42] A.S. Bakai, A.N. Timoshevskii, B.Z. Yanchitsky, On chemical bonding and helium distribution in hcp beryllium, Low Temp. Phys. 37 (9–10) (2011) 791–797.
[43] C. Stihl, R. Kumar, P.V. Vladimirov, A. Möslang, A multiscale study of the production and recombination of closely correlated defects from irradiation-induced higher order recoils in beryllium, Comput. Mater. Sci. 195 (2021) 110403.
[44] V. Chakin, R. Rolli, R. Gaisin, U. Hoeppener-Kramar, M. Nakamichi, M. Zmitko, Tritium release and retention in beryllium and titanium beryllide after neutron irradiation up to damage doses of 23-38 dpa, Fusion Eng. Des. 161 (2020) 111938.
[45] V. Chakin, R. Rolli, A. Moeslang, P. Kurinskiy, Tritium and helium release from highly neutron irradiated titanium beryllide, Fusion Eng. Des. 98-99 (2015) 1728–1732.